analytical chemistry

pubs.acs.org/ac Article

# Direct Current Electrokinetic Particle Trapping in Insulator-Based Microfluidics: Theory and Experiments

Braulio Cardenas-Benitez, Binny Jind, Roberto C. Gallo-Villanueva, Sergio O. Martinez-Chapa, Blanca H. Lapizco-Encinas, and Victor H. Perez-Gonzalez*

Cite This: *Anal. Chem.* 2020, 92, 12871−12879 Read Online

ACCESS | Metrics & More | Article Recommendations | Supporting Information

**ABSTRACT:** The classic theory of direct-current (DC) insulator-based dielectrophoresis (iDEP) considers that, in order to elicit particle trapping, dielectrophoretic (DEP) velocity counterbalances electro-kinetic (EK) motion, that is, electrophoresis (EP) and electro-osmotic flow (EOF). However, the particle velocity DEP component requires empirical correction factors (sometimes as high as 600) to account for experimental observations, suggesting the need for a refined model. Here, we show that, when applied to particle suspensions, a high-magnitude DC uniform electric field induces nonlinear particle velocities, leading to particle flow reversal beyond a critical field magnitude, referred to as the EK equilibrium condition. We further demonstrate that this particle motion can be described through an exploratory induced-charge EP nonlinear model. The model predictions were validated under an insulator-based microfluidic platform demonstrating predictive particle trapping for three different particle sizes (with an estimation error < 10%, not using correction factors). Our findings suggest that particle motion and trapping in "DC-iDEP" devices are dominated by EP and EOF, rather than by DEP effects.

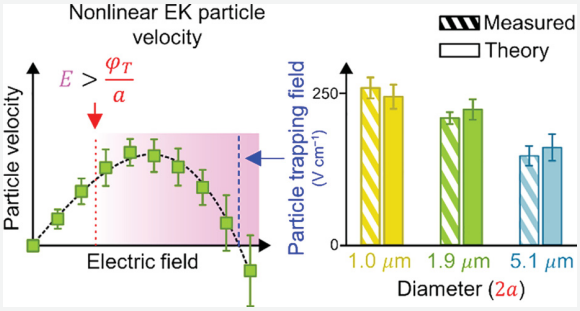




When a charged particle is suspended in an electrolyte solution, an electric double layer (EDL) forms at its solid/liquid interface with a potential, relative to the liquid bulk, in the order of the thermal voltage, $\varphi_T$ (~25 mV at room temperature).[1] Electrokinetic (EK) particle manipulation becomes possible through an externally applied electric field ($E_0$) that interacts with this EDL and the particle itself. The linear EK theory typically assumes that the potential drop over the length scale of the particle is much smaller when compared with $\varphi_T$ (i.e., $aE_0 \ll \varphi_T$, where $a$ is the particle radius). However, as applied fields grow in magnitude, they modify the spherically symmetric EDL of the particles—inducing a concentration polarization on the diffuse layer that sharply deviates from electroneutrality[2]—giving rise to induced-charge electrokinetics (ICEK).[1] These nonlinear processes,[2,3] which are intensified for highly conductive particles (relative to their suspending media) with nonzero Dukhin numbers,[4,5] arise from the effects of the typically ignored surface conductance.[6,7] While linear EK models have successfully explained the behavior of many microfluidic systems,[8] other phenomena naturally lay outside the realm of small applied electric fields.

In direct-current (DC) insulator-based dielectrophoresis (iDEP), nonuniform electric fields—typically in excess of 100 V cm$^{-1}$—are used to manipulate particle motion within microfluidic devices.[9−12] These devices have been modeled considering that particle trapping results from the interaction of electrophoresis (EP), electro-osmotic flow (EOF), and "dominant" dielectrophoresis (DEP)—with EP and EOF effects combining into an EK particle velocity term. This research field has grown considerably during the last two decades with new schemes being continually developed to enhance its selectivity and level of discrimination.[12−14] In principle, the design and modeling of iDEP systems could be used to predict the operating conditions required to achieve particle trapping. In practice, correction factors (sometimes as high as 600) have been empirically introduced to the theory, not to predict, but to account for the observed phenomena.[15] For instance, correction factors have been used in curvature-induced iDEP[16−18] and reservoir-based iDEP[19,20]—two variants of the original iDEP concept—in streaming[21,22] and trapping[11,23] applications and in the description of the "trapping value" parameter, which accounts for the trapping capacity of iDEP-based devices.[14,24,25] Importantly, these factors have been used not only in iDEP[15] but also in EOF and AC-EO pumps.[1]

**Received:** March 25, 2020
**Accepted:** September 7, 2020
**Published:** September 7, 2020





https://dx.doi.org/10.1021/acs.analchem.0c01303
*Anal. Chem.* 2020, 92, 12871−12879

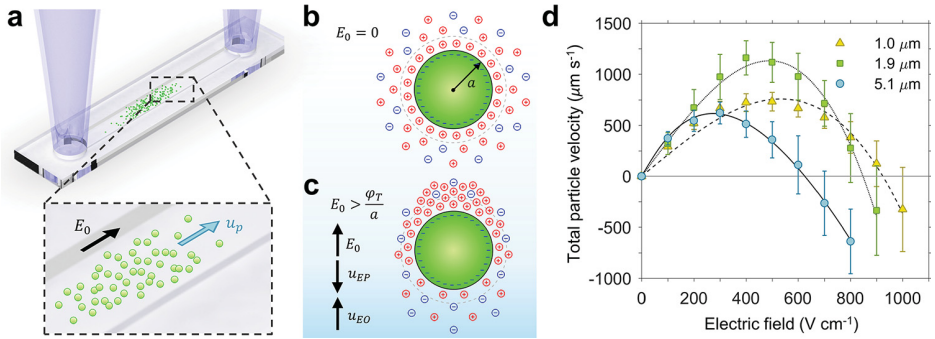


**Figure 1.** (a) Schematic of the microfluidic channel used to test the total velocity of carboxylated polystyrene microparticles subject to a uniform electric field. (b) Equilibrium EDL on a carboxylated microparticle ($E_0 = 0$). (c) Concentration polarization of the EDL upon application of a strong $E_0$. (d) Total particle velocity as a function of applied electric field, measured for three different particle sizes using particle tracking velocimetry (PTV).

The use of correction factors is not the only debatable aspect in the iDEP-based microfluidics literature. A contradiction in the interpretation of experimental observations is evident when comparing electrode-based DEP (eDEP) with iDEP works. Under the same set of experimental conditions (i.e., dielectric beads, suspending solution dielectric properties, and in the limit of zero frequency fields), works on eDEP report positive DEP,[26] while works on iDEP report negative DEP.[12] In a DEP experiment, prediction of particle trapping requires the a priori determination of the Claussius−Mossotti factor ($f_{CM}$) from previously calculated particle ($\sigma_p$) and medium ($\sigma_m$) conductivities. However, because only $\sigma_m$ can be directly measured, the few reports that predict or describe DC-iDEP trapping either assume low $\sigma_p$ values when compared with $\sigma_m$ (resulting in $f_{CM} < 0$)[27] or set $\sigma_p = 0$, under the argument that negative DEP must be opposing EK velocity.[11] Consequently, the majority of DC-iDEP studies present a posteriori analyses of the trapping conditions, where $f_{CM} < 0$ is implied.[9,14,28,29]

In this paper, we study the EK velocity of carboxylated dielectric spheres of different diameters (1.0, 1.9, and 5.1 $\mu$m) subjected to a DC uniform electric field (absent DEP, see Figure 1a). We then use this information to predict particle trapping under a DC nonuniform electric field (in the presence of DEP). Using previously derived EP models,[4,5] we explain the experimentally observed EK particle velocities using higher-order terms. We observed that, although particles follow the direction of EOF under low-magnitude uniform fields, they reverse their motion beyond a critical electric field magnitude, deemed the EK equilibrium condition ($E_{EEC}$) of the particle. Furthermore, we found that $E_{EEC}$ magnitudes provide a fair estimate of trapping conditions under nonuniform fields. Our model can therefore be used to predict the conditions needed to elicit particle enrichment (within a < 10% error margin), and to extract particle properties without artificially introduced correction factors. Remarkably, these findings suggest that particle motion in "DC-iDEP" devices is dominated by EP and EOF, rather than DEP.

## THEORY AND COMPUTATIONAL MODEL

**Nonlinear Electrophoretic Velocity.** Consider a dielectric particle of radius $a$, and surface charge density $\rho_q$, immersed in an infinite symmetric electrolyte with valency $\pm Z$ (with corresponding ionic diffusivities of $D_+$ and $D_-$), conductivity $\sigma_m$, equilibrium concentration $n_0$, permittivity $\epsilon_m$, and viscosity $\eta$. Here, the thermal voltage is defined as $\varphi_T = k_B T/Ze$, where $k_B$ is the Boltzmann constant, $T$, the temperature of the system, and $e$, the elementary charge. Such system is shown in Figure 1b, where the Debye length is given by $\kappa^{-1} = \sqrt{\frac{\epsilon_m \varphi_T}{2Zen_0}}$. In a reference frame where the particle is fixed at the origin, a uniform field of magnitude $E_0$ is applied, pointing in the positive $y$-axis direction and producing a relative flow field ($\mathbf{u}$) surrounding the particle. In what follows, we use the EK model by Schnitzer and Yariv (SY model[4,5]) to calculate flow velocity far from the described particle, that is, $\mathbf{u} \rightarrow -u_{EP}\hat{\mathbf{j}}$ as $|r| \rightarrow \infty$, where $u_{EP}$ is by definition the electrophoretic velocity in terms of $E_0$.

The SY model assumes stationary Stokes flow (Re $\ll 1$) and a thin EDL ($\kappa a \gg 1$). Application of the weakly nonlinear version of the SY model[5] allows calculating $u_{EP}$ far from the highly charged particle surface—a condition fulfilled when the particle surface charge density compares to $2Zen_0a$ (around $\pm 0.05-0.5$ $\mu$C cm$^{-2}$ for a micron-sized particle immersed in a monovalent salt solution with concentration between 5 and 50 $\mu$M). Notice the charge condition is readily fulfilled for negatively charged carboxylated polystyrene beads ($-1.41 \sim -5.93$ $\mu$C cm$^{-2}$).[30] Introducing the dimensionless ionic drag coefficient $\alpha^{\pm} = \epsilon_m \varphi_T^2/\eta D_{\pm}$, the system nonlinearity can be described through the modified Dukhin number:[5]

$$\mathrm{Du} = (1 + 2\alpha^+)\frac{\rho_q}{2Zen_0a} \tag{1}$$

A perturbation approach at $\sim O(E_0^3)$ in the weak-field limit ($\frac{E_0}{\beta} \sim O(1)$, where $\beta = \varphi_T/a$ is the characteristic field strength) allows calculation of $u_{EP}$ in terms of Du:[5]

$$u_{EP} = \mu_{EP}^{(1)} E_0 + \mu_{EP}^{(3)} E_0^3 \tag{2}$$

where the first- and third-order mobilities are given by

$$\mu_{EP}^{(1)} = -\frac{\epsilon_m \varphi_T}{\eta}\left(\frac{\zeta_0 + \mathrm{Du}\cdot\ln(16)}{1 + 2\mathrm{Du}}\right) \tag{3}$$

$$\mu_{EP}^{(3)} = -\frac{a^2 \epsilon_m}{\eta \varphi_T} f(\mathrm{Du}, \zeta_0, \alpha, \grave{\alpha}) \tag{4}$$

with dimensionless particle zeta potential $\zeta_0 = 2\ln\left(\frac{\rho_q}{\epsilon_m \kappa \varphi_T}\right)$, dimensionless coefficients $\alpha = (\alpha^+ + \alpha^-)/2$ and $\grave{\alpha} = (\alpha^+ - \alpha^-)/2$, and $f(\mathrm{Du}, \zeta_0, \alpha, \grave{\alpha})$ is defined as a nonlinear function of


https://dx.doi.org/10.1021/acs.analchem.0c01303
Anal. Chem. 2020, 92, 12871−12879

the particle's EK properties. Alternatively, the case for arbitrary $E_0$ and small (but finite) Du can be represented by a variant of the SY model,[4] which gives a different $E_0$ dependence:

$$u_{EP} = \frac{\epsilon_m \varphi_T^2}{\eta a}(\zeta_0 E_0 + \mathrm{Du}\mathcal{U}_1) \tag{5}$$

where $\mathcal{U}_1$ is a nonlinear function that varies as $\sim E_0^{3/2}$ for large applied fields ($E_0 \gg \beta$). The above eqs 2−5 allow calculating the EP velocity for a particle immersed in a quiescent fluid. To extend these equations to the case of combined EP and EO motion, one can use the linearity and superimposability of the Stokes equation to conclude that the total flow field far from the particle is the combined EO + EP components.[31] This is achieved by considering the EOF (absent the particle) and superposing it with the EP flow caused by the particle, provided that the distance between the particle and any of the walls is much greater than $\kappa^{-1}$. Under these assumptions, the total particle velocity with respect to the fixed microchannel frame of reference ($u_p$) becomes

$$u_p = u_{EP} + u_{EO} \tag{6}$$

where $u_{EP}$ is given by either eq 2 or eq 5 depending on the approximation taken, and $u_{EO} = -\frac{\epsilon_m \zeta_w}{\eta} E_0$, where $\zeta_w$ is the zeta potential of the polydimethylsiloxane (PDMS) walls. We assume the magnitude of $u_{EO}$ grows linearly, since for a planar PDMS wall, the surface conductance effects will be greatly reduced (Du → 0 as the radius of curvature grows). Figure 1c depicts the EDL distortion as well as the EOF and nonlinear EP velocities with respect to the microfluidic channel fixed reference frame (rather than the particle frame), to directly compare them against the experimentally measured $u_p$. Taking the approximation in eq 2 and setting $u_p = 0$ in eq 6 allows an explicit computation of the electrokinetic equilibrium condition:

$$E_{EEC} = \sqrt{-\frac{\mu_{EP}^{(1)} + \mu_{EO}}{\mu_{EP}^{(3)}}} \tag{7}$$

which we define as the electric field magnitude required to balance the EO velocity component with the nonlinear EP. In addition to showing the interplay between the mobilities involved in reaching EK equilibrium, division by the square root of $\mu_{EP}^{(3)}$ in eq 7 indicates the inverse relationship between $E_{EEC}$ and $a$, in agreement with our observations, as will be detailed in the Results and Discussion section. For eqs 2 and 5, calculations of $f(\mathrm{Du}, \zeta_0, \alpha, \grave{\alpha})$, and $\mathcal{U}_1$ are given in the Supporting Information.

**Nonuniform Electric Field.** Particles were tested in two different microchannel geometries: one with no posts (Figure 1a) for performing the $E_{EEC}$ experiments at uniform $E_0$ and the other with a two-post geometry at the middle section (Figure 2a, inset), which allowed us to introduce a field nonuniformity to capture particles. The second case admits a representation in the bipolar system of coordinates (Figure S3) in which the Laplace equation is separable.[32] We have derived the analytic expression for this **E** field within the microchannel by approximating the two-post geometry as two dielectric circles of permittivity $\epsilon_{in}$ and diameter $D$ separated by a distance $G$, immersed in an infinite 2D medium with permittivity $\epsilon_m$. It can be shown that **E** is fully determined by the gap-to-post diameter ratio, $\gamma = G/D$, and by $q = \epsilon_{in}/\epsilon_m$. In fact, we found

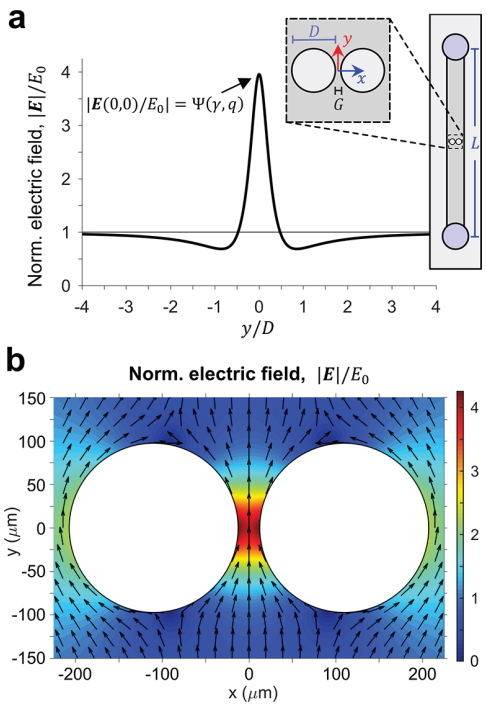


**Figure 2.** (a) Plot of the normalized electric field along the $x = 0$ axis of microdevices. Inset: microfluidic device with two insulating circular posts $G = 25$ μm, $D = 200$ μm, and $L = 1$ cm. (b) Normalized electric field distribution near the two insulating posts.

that Eq. (S21) in the Supporting Information is the general form of the previously reported case of perfectly insulating cylinders ($q \to 0$ in ref 32.).

To analyze the electric field that particles experience as they travel through the dielectric constriction, an expression for $\mathbf{E}(0, y)$ can be obtained analytically:

$$\mathbf{E}(0, y) = E_0\left[1 - \frac{8}{1 + \left(\frac{y}{\bar{a}}\right)^2}\mathrm{Re}\left\{\sum_{m=1}^{\infty} \frac{m\left(\frac{y - i\bar{a}}{y + i\bar{a}}\right)^m}{g(\gamma)^{2m}\left(\frac{1+q}{1-q}\right) - 1}\right\}\right]\hat{\mathbf{j}}$$
$$= E_0 Y(y, \gamma, q)\hat{\mathbf{j}} \tag{8}$$

where $\bar{a}$ is the circle foci coordinate in bipolar coordinates, $i = \sqrt{-1}$, and $g(\gamma)$ is a function of geometry (See eq. S24 in the Supporting Information). Function $Y(y, \gamma, q)$ therefore encodes the field amplification at $y$ (Figure 2a). The maximum field magnitude along $x = 0$ happens at the origin and is proportional to $E_0$ times a function of $\gamma$ and $q$:

$$\mathbf{E}(0, 0) = E_0\left[1 - 8\sum_{m=1}^{\infty} \frac{m(-1)^m}{g(\gamma)^{2m}\left(\frac{1+q}{1-q}\right) - 1}\right]\hat{\mathbf{j}}$$
$$= E_0 \Psi(\gamma, q)\hat{\mathbf{j}} \tag{9}$$

where the function $\Psi(\gamma, q)$ is deemed the DC field-independent amplification factor of the system. Taking $\epsilon_{in} \sim 2.3$−$2.8$ for PDMS[33] and $\epsilon_m \sim 80$ for diluted electrolytes results in $q \ll 1$, and thus, we implemented $q = 0$ in our analytic model.

In addition to the analytical electric field model, we computed two 2D finite element models using COMSOL


https://dx.doi.org/10.1021/acs.analchem.0c01303
Anal. Chem. 2020, 92, 12871−12879

Multiphysics 5.2, which are both detailed in the Supporting Information. The first one served as a numerical validation of the analytical model by approximating the geometry as two dielectric circles in a semi-infinite plane (Figure S4). The second simulation, shown in Figure S5, was computed to better approximate the complete 2D geometry in Figure 2a (inset).

**Dielectrophoresis Model.** The classic iDEP hypothesis, based on linear EK, indicates that particle trapping within a device with dielectric constrictions will occur where the magnitude of the DEP velocity ($\mathbf{u}_{DEP}$) matches the EK velocity ($\mathbf{u}_{EK}$). In this scenario, $\mathbf{u}_{DEP}$ is given by $\mu_{DEP} \nabla (\mathbf{E}\cdot\mathbf{E})$, where the mobility is $\mu_{DEP} = a^2\epsilon_m f_{CM}/3\eta$ and $f_{CM} = (\sigma_p - \sigma_m)/(\sigma_p + 2\sigma_m)$ in the DC regime. Here, particle conductivity is defined as[34]

$$\sigma_p = \sigma_b + 2K^\sigma/a \tag{10}$$

where $\sigma_b$ is the bulk conductivity of the particle ($\sigma_b \sim 0$ for polystyrene). Moreover, the EK velocity, $\mathbf{u}_{EK} = \mu_{EK}\mathbf{E}$, is dictated by the linear relationship $\mu_{EK} = \epsilon_m(\zeta_p - \zeta_w)/\eta$, where the particle zeta potential is $\zeta_p = \varphi_T\zeta_0$. If $f_{CM} > 0$, the iDEP hypothesis predicts particle migration toward the device's constriction (i.e., regions where $\mathbf{E}$ is maximum), whereas $f_{CM} < 0$ predicts particle repulsion from such regions. Negative DEP would consequently result in particles being trapped slightly before the center of the constriction, where $|\mathbf{u}_{EK}| = |\mathbf{u}_{DEP}|$, giving rise to the iDEP immobilization criterion:

$$\mu_{EK}\mathbf{E}\cdot\mathbf{E} + C\mu_{DEP}\nabla(\mathbf{E}\cdot\mathbf{E})\cdot\mathbf{E} = 0 \tag{11}$$

where $C$ is the typically introduced empirical correction factor that accounts for phenomena not included in that model.[15]

## EXPERIMENTAL SECTION

**Microparticle Preparation.** Carboxylated latex beads of diameters of 1.0, 1.9, and 5.1 $\mu$m were purchased from Invitrogen and Magsphere (F8823 and F8827; Invitrogen, Carlsbad, CA, and CAYF-005UM; Magsphere Inc., Pasadena, CA, respectively). The 5.1 $\mu$m particle suspension was washed by centrifugation three times for 2 min at 5000 rpm to remove its preservative sodium azide. The three particle sizes were diluted to a concentration of $\sim 1 \times 10^6$ microspheres/mL in deionized water. Appropriate amounts of KCl—6.5, 14.8, and 53.3 $\mu$M, respectively—were added to each solution to satisfy the thin EDL condition ($\kappa a > 10$)[34] and to minimize Joule heating ($\sigma_m < 10$ $\mu$S cm$^{-1}$).[35]

**Microdevice Fabrication.** PDMS microdevices were fabricated by conventional soft lithography.[35] For each $E_{EEC}$ experiment of a given particle size, three copies were made with length $L$ = 1 cm, width $w$ = 1 mm, and height $H$ = 19.6 $\mu$m. This method was also used to obtain triplicate copies of devices with circular posts (dimensions and protocols can be found in the Supporting Information, Table S1).

**Electrokinetic Equilibrium Condition Experiments.** Before EK experiments, PDMS microchannels were subjected to 5 min of vacuum followed by priming with deionized water. After priming, bubbles were allowed to degas out of the devices (~10 min) followed by 1 h of waiting to allow for the new media to settle within the devices. For each of the three solutions, particles were sonicated for 2 min and then introduced by means of large volume inlet/outlet reservoirs (~2 mL, Figure S1). A high-voltage sequencer model HVS6000D (LabSmith, Livermore, CA) was used to apply a series of DC voltages between the two reservoirs using platinum electrodes and an automated routine (see the Supporting Information). The applied voltage $V_0$ was increased in steps of 100 V from 0 to 800, 900, and 1000 V for the 1.0, 1.9, and 5.1 $\mu$m particles, respectively, until clear particle flow reversal was observed. The complete sweep was recorded on a Nikon Eclipse Ti2-E inverted microscope (Nikon Instruments Inc., NY, USA) at 20 fps (~50 ms exposure, ROI ~ 1300 × 1300 $\mu$m) and processed using ImageJ. Each voltage in the sweep was applied three times. For all voltage applications, the y-axis velocity of 10 randomly selected particles was tracked and averaged over 10 frames. The complete assay was performed in triplicate per particle size using a new device and fresh media each time. Additionally, each particle solution was tested in an independent control experiment in which the particle velocity was recorded upon a first application of a high-voltage signal (2000 V, see Movie S4).

**Particle Trapping Experiments.** Using the devices with circular posts, we followed the same priming procedure and solutions as in the $E_{EEC}$ protocol. Since a lower applied field is needed to elicit particle trapping than that needed to obtain $E_{EEC}$, the voltage sweep was adapted to a lower range. The applied field $E_0 = V_0/L$ was increased in steps of 25 V cm$^{-1}$ (starting at 100 V cm$^{-1}$), until the first trapping field $E_{trap} = V_{trap}/L$ was identified; afterward, steps of 50 V cm$^{-1}$ were used until reaching ~$2E_{trap}$ (see the Supporting Information for details). Field applications were repeated three times at each step. ImageJ was used to measure the trapping position of particles along the $y$-axis of channels ($y_{trap}$). After one sweep, the complete assay was repeated two more times using new devices and solutions.

## RESULTS AND DISCUSSION

**Particle Velocity as a Function of Electric Field.** To investigate particle behavior as a function of electric field, we prepared three different microparticle solutions with green fluorescent carboxylated polystyrene beads of different sizes (1.0, 1.9, and 5.1 $\mu$m), each of which was loaded into a straight PDMS microfluidic device (Figure 1a). The DC voltage $V_0$ across the conductive fluid filling the channel produces a uniform field $E_0 = V_0/L$ in the middle portion of the channel. Using particle tracking velocimetry (PTV), we tracked the particles' migration to determine the combined effects of EOF and EP on them (i.e., to measure their EK velocity or their total velocity $u_p$). Figure 1d shows the dependence of $u_p$ with $E_0$ for the three particle sizes. Four characteristic domains for $u_p$ were identified: (i) at low fields, $u_p$ followed a linear response,[36] in agreement with the classical EK theory $u_{EP} \sim O(E_0)$ (Smoluchowski's velocity equation);[37] (ii) beyond the linear regime ($E_0 \gtrsim \beta$), $u_p$ reached a maximum value $u_{max}$ ; (iii) after the apex, $u_p$ decreased until reaching an unstable equilibrium near zero—the EK equilibrium condition, that is, $u_p(E_{EEC}) = 0$; and (iv) a region where $E_0 > E_{EEC}$ that resulted in particles reversing their original direction (Movies S1, S2, and S3).

To confirm the velocity reversal at a high $E_0$, we further tested particles at 2000 V cm$^{-1}$ without applying any prior electric field. We observed that particles immediately (<50 ms) migrated opposite to the EOF direction, instead of following the applied field direction (i.e., toward the anode, see Movie S4). The resulting negative velocities of −2609, −3408, and −6442 $\mu$m s$^{-1}$ for 1.0, 1.9, and 5.1 $\mu$m particles, respectively,


https://dx.doi.org/10.1021/acs.analchem.0c01303
Anal. Chem. 2020, 92, 12871−12879

Table 1. Electrokinetic Properties for the Three Particle Sizes, along with the Medium Properties and the Measured EK Equilibrium Condition Values ($E_{EEC}$)[a]

| particle diameter ($\mu$m) | charge ($\mu$equiv g$^{-1}$)[b] | pH | $c_0$ ($\mu$M) | $\sigma_m$($\mu$S cm$^{-1}$) | $\kappa^{-1}$ (nm) | $\zeta_w$ (mV) | charge density, $\rho_q$ ($\mu$C cm$^{-2}$) | $\sigma_p$ ($\mu$S cm$^{-1}$) | $R^2$ | Du | $E_{EEC}$(V cm$^{-1}$) |
|---|---|---|---|---|---|---|---|---|---|---|---|
| 1.0 | 182.6 | 5.7 ± 0.1 | 53.3 ± 0.1 | 8.35 ± 0.01 | 42 | −83 ± 1 | −0.71 ± 0.16 | 21.81 ± 4.92 | 0.964 | 2.11 | 942.3 ± 77.3 |
| 1.9 | 24.6 | 5.6 ± 0.2 | 14.8 ± 0.1 | 3.06 ± 0.01 | 79 | −101 ± 3 | −0.13 ± 0.01 | 2.09 ± 0.16 | 0.990 | 0.73 | 851.6 ± 67.3 |
| 5.1 | 7.0 | 5.5 ± 0.1 | 6.5 ± 0.1 | 1.54 ± 0.01 | 120 | −85 ± 1 | −0.10 ± 0.01 | 0.63 ± 0.06 | 0.998 | 0.22 | 629.4 ± 81.4 |

[a]The $\kappa^{-1}$ and Du values were calculated from measured data. Error values for $\zeta_w$, $\rho_q$, and $\sigma_p$ represent the 95% confidence intervals obtained by fitting particle velocity to eq 6. Concentrations are related to $n_0$ by $c_0 = n_0/N_A$, where $N_A$ is Avogadro's number. [b]Obtained from the manufacturer.

Table 2. Predictions of $E_{trap}$ Using Three Different Models (P1−P3)[a]

| particle diameter, ($\mu$m) | P1: DEP theory (V cm$^{-1}$) | P1: correction factor, $C$ | P2: nonlinear EK, analytic (V cm$^{-1}$) | P2: field Amp. factor, Ψ | P3: nonlinear EK, COMSOL (V cm$^{-1}$) | measured $E_{trap}$, (V cm$^{-1}$) | error % in P2 (analytic) | error % in P3 (COMSOL) |
|---|---|---|---|---|---|---|---|---|
| 1.0 | 73,005 | 285.62 | 241.3 ± 19.8 | 3.91 | 243.8 ± 20.0 | 255.6 ± 16.7 | 5.91 | 4.81 |
| 1.9 | 28,260 | 137.45 | 219.6 ± 17.3 | 3.88 | 221.8 ± 17.5 | 205.6 ± 11.0 | 6.39 | 7.31 |
| 5.1 | 3395 | 23.51 | 159.0 ± 20.6 | 3.96 | 160.6 ± 20.8 | 144.4 ± 16.7 | 9.15 | 10.06 |

[a]P1 is the estimated $E_{trap}$ assuming a DEP theory with linear EK ($f_{CM} = -1/2$, and $\sigma_p = 0$). Ψ is calculated using device geometry (see Table S1). P2 and P3 are the estimated $E_{trap}$ using eq 9 and the COMSOL simulations, respectively.

support the hypothesis that increased EP, rather than permanent changes in the medium affecting EOF, originates from the nonlinear EK response. We note this applied $E_0$ magnitude is within typical values in DC-iDEP (150−4000 V cm$^{-1}$).[12,38,39] These nonlinear velocity results suggest that strong uniform electric fields produce an unaccounted-for particle velocity component greater than $u_{EO}$. In what follows, we apply the SY model to $u_p$ data as an exploratory model to understand the nonlinear functions in Figure 1d.

**Application of Nonlinear Electrokinetic Theory to Experimental Particle Velocity Data.** Using eq 6, we performed nonlinear least-squares fitting of the data in Figure 1d with $\zeta_w$ and $\rho_q$ as fitting parameters (since $\zeta_w$ varied with the different particle media and $\rho_q$ changed depending on the particle). Results are summarized in Table 1, along with the measured particle and medium EK properties and $E_{EEC}$ values; details of the physical parameters used to compute eqs 2−6 can be found in Table S2. We found that the triplicate experiments per particle size yielded a variation of $\zeta_w$ between −83 and −101 mV, which are expected values for diluted media[40] and for PDMS below pH = 7.[41] Although reservoirs within the mL range greatly mitigate pH changes,[40] the ∼22% variation in $\zeta_w$ could have arisen from using a low conductivity, nonbuffered KCl solution—a condition necessary to minimize Joule heating and maintain a symmetric electrolyte in our experimental and theoretical design.

To compare data with reported values, the fitted $\rho_q$ can be translated into surface conductance by approximating $K^\sigma \sim \mu_s^+\rho_s$ and assuming $\rho_s \sim \rho_q$, where $\mu_s^+$ is the counterion mobility ($7.69 \times 10^{-8}$ m$^2$ V$^{-1}$ s$^{-1}$ for K$^+$) and $\rho_s$ is the Stern layer surface charge density.[34] For the 1.0 and 1.9 $\mu$m particles, eq 2 yielded the best results in terms of both $R^2$ and the obtained fit parameters. Although a good fit was obtained for 5.1 $\mu$m particles using eq 2, the obtained $K^\sigma$ values (∼0.04 nS) were lower than those typically reported (∼1 nS).[34] Conversely, the use of eq 5 produced an overall better fitting quality ($R^2$= 0.998) with more realistic $K^\sigma$ values (∼0.1 nS). Our computed $K^\sigma$ values range between 0.1 and 0.55 nS for medium conductivities of 1.54−8.35 $\mu$S cm$^{-1}$, which are closely related to the properties of latex particles measured by electrorotation that place $K^\sigma$ between 0.2 and 2.1 nS for $\sigma_m \sim$ 2−16 $\mu$S cm$^{-1}$.[42] Furthermore, the relatively low fitted $\rho_q$ values can be explained by comparing them to the reported charge by the manufacturer, which for the lowest case (7.0 $\mu$equiv g$^{-1}$) translates to $-0.3 \sim -1.2$ $\mu$C cm$^{-2}$, considering the speciation of carboxyl groups[43] ($pK_a$ = 5.8 ± 0.3) at the measured pH value of 5.5.

The problem of choosing the correct fit equation, eqs 2 or 5, is nontrivial because there exists no current analytically tractable expression for $u_{EP}$ that fully describes the regime $E_0 \gtrsim \beta$ for Du $\gtrsim$ 1. Therefore, the application of eq 2 remains strictly exploratory. Because most EK particle trapping experiments work in that complex range, a challenge exists in connecting experimental data with the currently available theory. For 5.1 $\mu$m particles, $\beta$ is as low as 98 V cm$^{-1}$, while for 1.9 and 1.0 $\mu$m particles, $\beta$ increases to 265 and 500 V cm$^{-1}$, respectively. Here, the tested field ranges correspond to 0−800 V cm$^{-1}$ for 5.1 $\mu$m, 0−900 V cm$^{-1}$ for 1.9 $\mu$m, and 0−1000 V cm$^{-1}$ for 1.0 $\mu$m particles, representing fields in the order of 8.16, 3.42, and 2$\beta$. Evidently, 5.1 $\mu$m particles present the largest deviation from $\beta$, possibly explaining why the fitting at $\frac{E_0}{\beta} \sim O(1)$ and arbitrary Du from eq 2 fails, while the arbitrary $E_0$ approach of eq 5 gives the overall best fit results. In addition, to determine the suitable approximation, a good estimate of $\rho_q$ is required prior to performing the functional fit. We found that using the electrical charge reported by the manufacturer can serve as a fair starting point for choosing the functional form of $u_{EP}$ (5.1 $\mu$m particles possess the lowest charge, see Table 1). Regardless of the model used to describe $u_p$ in the experimentally tested field ranges, the functional behavior found through the electric field parametric study serves as a quantitative model that predicts $E_{EEC}$.

**Particle Trapping: The iDEP Hypothesis Versus the Nonlinear Electrokinetic Hypothesis.** We evaluated the analytical electric field model to predict the nonuniform **E** distribution in the particle trapping experiments. Figure 2a depicts evaluation of eq 8, which shows an amplification of Ψ ∼ 4, while Figure 2b represents the obtained normalized 2D field distribution. Table 2 summarizes the different amplification factors calculated for the microdevices used in each of the particle trapping experiments (variations stem from the slight geometric differences in the devices, see Table S1).


https://dx.doi.org/10.1021/acs.analchem.0c01303
Anal. Chem. 2020, 92, 12871−12879

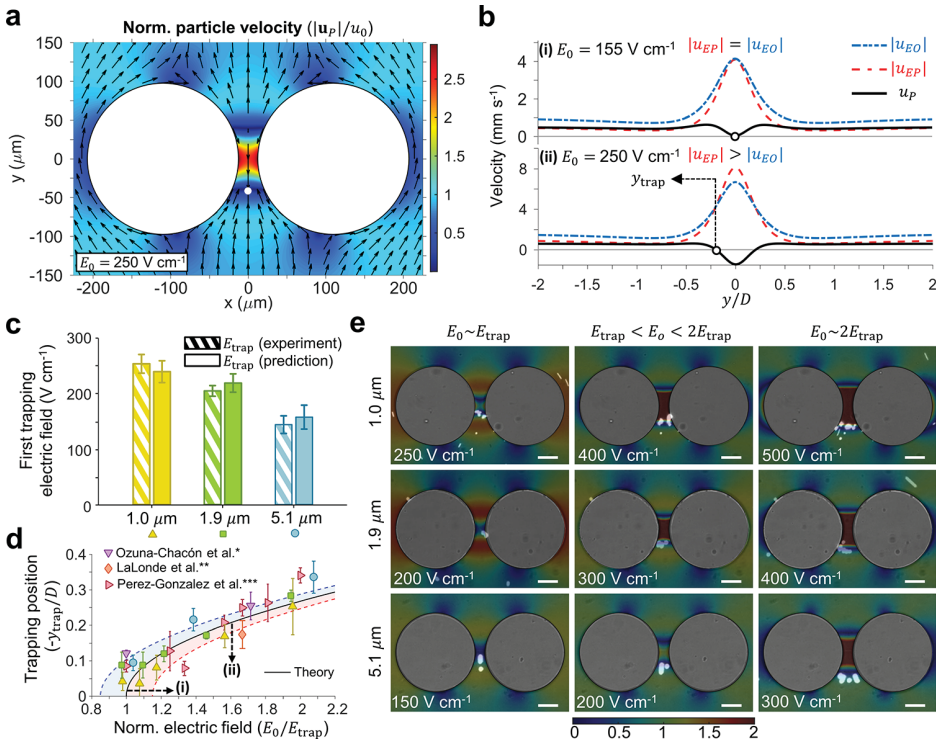


**Figure 3.** (a) Predicted normalized particle velocity for 5.1 $\mu$m particles at $E_0$ = 250 V cm$^{-1}$. Color map normalized to the particle velocity at uniform $E_0$ = 250 V cm$^{-1}$ (see velocity plots in Figure 1d); a small white dot shows the trapping position. (b) Velocity cutline plots along $x$ = 0; (**i**) particle velocity at $E_0 \sim E_{trap}$($E_0$ = 155 V cm$^{-1}$) and (**ii**) particle velocity beyond $E_{trap}$. (c) Predicted versus experimental $E_{trap}$, for all particle sizes. (d) Trapping position along the negative y-axis as a function of $E_0$ normalized by $E_{trap}$. Theoretical line obtained from eq 8, with dashed lines showing a ± 15% variation. Additional data taken from previous works for comparison: * and ** data from circular post geometries ($D$ = 400 $\mu$m[51] and 200 $\mu$m,[52] respectively) for 1 $\mu$m particles; *** data from elliptic posts normalized by post length along $y$-axis ($D$ = 75 $\mu$m)[38] and for 1 $\mu$m particles. (e) Superimposition of the microparticle trapping fluorescence images and the 2D normalized total particle velocity distributions. Rows show trapping by particle size, and columns display the different applied fields (scale bars 50 $\mu$m).

The analytic **E** equation can be used to forecast the field necessary to elicit the first particle trapping event, $E_{trap} = V_{trap}/L$. The DEP and nonlinear EK theories, however, offer very different estimations. As seen in Table 2, evaluating eq 11—the DEP and linear EK model, see Figure S6—resulted in high $E_{trap}$ predictions in excess of 3 kV cm$^{-1}$, even for the maximum possible repulsive force, that is, $\sigma_p = 0$, $f_{CM} = -1/2$ (with no correction, $C = 1$). Measuring $E_{trap}$ allows an a posteriori determination of $C$. An adjustment of $C$ = 23.51 in eq 11 for 5.1 $\mu$m particles was found to be commensurate with values in the literature.[9,10,15] For 1.0 $\mu$m particles, a correction of $C$ = 285.62 indicated a two order of magnitude difference between $\mu_{DEP}$ and $\mu_{EK}$, comparable to previous works.[11] Furthermore, the case $\sigma_p \neq 0$, typically evaluated in the literature by assuming $K^{\sigma} \sim 1$ nS in eq 10, resulted in either positive DEP or near to zero polarization($f_{CM} \sim 0$, not shown in Table 2), thus predicting negligible DEP forces and no possible trapping in DC mode.

In contrast to the iDEP model, the nonlinear EK hypothesis suggests that, if the spatial variations of the **E** within the microfluidic device are small enough when compared with $a$ and $\kappa^{-1}$, the particles would halt in the regions where two conditions are met: (i) where $|\mathbf{E}| = E_{EEC}$, as $\mathbf{u}_p$ would be zero under the applied field and (ii) where $\nabla \cdot \mathbf{u}_p < 0$. For the first condition to be fulfilled, nonlinear EK effects have to be strong enough to counteract the EOF—a requirement that is satisfied in the presented EK experiments (Du ≠ 0 and $E_0 \gtrsim \beta$). The second condition is met at points where the particle velocity vector field is not divergent. Taking the experimentally determined $E_{EEC}$ as the starting point of the nonlinear EK hypothesis (Table 1 and Figure 1d), we used eq 9 and the microchannel geometry data to calculate the $\Psi$ at the constriction generated by applying $E_{trap}$, viz. $\mathbf{E}(0,0) = E_{EEC}\hat{\mathbf{j}}$. As evidenced in Table 2, the experimental $E_{trap}$ values agree with predictions within at most 9.15% error. We further compared the analytical prediction against a finite element simulation using COMSOL Multiphysics (Table 2 and Table S1). Using this simulation, we calculated $\Psi$ values of 3.86, 3.84, and 3.92 (not included in Table 2) for the channel geometries used in the 1.0, 1.9, and 5.1 $\mu$m particle experiments, respectively. These amplifications resulted in prediction errors that differed from analytical predictions by <1.1%, as seen in Table 2.

Lastly, we experimentally tested the case $\sigma_m \gg \sigma_p$ for 5.1 $\mu$m particles—a condition under which, according to the iDEP hypothesis, particles should experience the strongest negative DEP force. However, no clear particle trapping was observed in those experiments. Moreover, for the $E_{EEC}$ test, particles displayed a highly linear response throughout the complete 0–800 V cm$^{-1}$ tested range (Figure S7). This behavior can be explained by considering the effect of low Du on eq 5. Since Du = 0.02 for this case, eq 5 predicts a linear response (no $E_{EEC}$ value), and thereby no trapping.

**Nonlinear Electrokinetic Trapping of Dielectric Particles.** We observed that particle trapping occurred approximately where the balancing of velocity components


https://dx.doi.org/10.1021/acs.analchem.0c01303
Anal. Chem. 2020, 92, 12871−12879

takes place ($\mathbf{u}_p = 0$), and where $\nabla \cdot \mathbf{u}_p < 0$. Starting from the fit equations in Figure 1d, one can use the bipolar conformal mapping (or a finite element simulation for an arbitrary geometry) to estimate the velocity distribution for a particle. Figure 3a presents a 2D plot of the normalized particle velocity $|\mathbf{u}_p(x, y, E_0)|/ u_0$ for 5.1 $\mu$m particles, with $u_0$ being the velocity of the particle with no field amplification, that is, $u_0 = u_p$ at $E_0$ = 250 V cm$^{-1}$. In this velocity map, a white dot shows the trapping position $y_{trap}$, where $\mathbf{u}_p(0, y_{trap}) = 0$ and the vector field portraits the velocity convergence condition. Additionally, Figure 3b displays a plot along $x = 0$ of Figure 3a, for two cases: (i) when the magnitude of $E_0$ is exactly enough for EP to counter balance EOF, that is, $|u_{EP}| = | u_{EO}|$ and ii) when $|u_{EP}| > | u_{EO}|$, which pushes the zero-crossing further down the negative values of the normalized $y$-axis. Notice that for trapping to occur, both conditions, $\mathbf{u}_p = 0$ and $\nabla \cdot \mathbf{u}_p < 0$, need to be met. For instance, Figure 3b; (ii) shows two zero-crossings, but Figure 3a demonstrates that for the second zero $\nabla \cdot \mathbf{u}_p > 0$, resulting in no trapped particles at that position. Evidently, particles with different EK properties will experience a characteristic zero-crossing—a microfluidic principle that has been exploited under the DC-iDEP hypothesis both to separate and to characterize cells by the polarizability of their envelope.[9,10]

Figure 3c provides further comparison between $E_{trap}$ values and those predicted by the mathematical model and additionally evinces the reduction of $E_{trap}$ with increase in the particle size. This behavior can be anticipated from eq 7, for which $E_{EEC}$ is inversely proportional to $a$. Once these trapping values were obtained, the applied $E_0$ can be extended in excess of $E_{trap}$, which results in particles receding from the first trapping position near (0,0). Figure 3d presents the magnitude of this normalized trapping position ($-y_{trap}/D$) for all tested particles, generated by the applied $E_0$ normalized by the first trapping field $E_{trap}$. For this figure, we computed the critical values of $-y_{trap}$, where the field equals $E_{EEC}$ (continuous line). This line represents the points at which $u_p = 0$, and thus, the conditions represented in Figure 3b (i) and (ii) map into it as indicated by the arrow marks. We have further shown how data in the literature are compared with this mapping within ±15% bounds (dashed lines). Although these values are not expected to exactly match the trapping relationship due to the different experimental conditions, they do offer a comparative view of the scaling behavior of $-y_{trap}/D$, where $D$ is taken as the post length along the $y$-axis.

To further depict the relationship found in Figure 3d, we obtained the 2D plots of the normalized velocity for all particles and superimposed them with the experimentally obtained fluorescence images of particle trapping (Figure 3e). For each particle size, three representative cases were selected: the first trapping fluorescent intensity picture at $E_0 \sim E_{trap}$, an intermediate value, and $E_0 \sim 2E_{trap}$. In those figures, approximates are shown because $E_{trap}$ was obtained from averaging the experimental trapping fields (see Table 2). In addition, the normalized velocity plots of Figure 3e were obtained by using the functional fits from Figure 1d and evaluating them at the displayed $E_0$. As evidenced, the predicted trapping zones are in excellent qualitative agreement with the experiments. Moreover, Figure 3d,e confirms that normalization of $E_0$ by $E_{trap}$ maps trapping points to similar locations despite particles having different sizes. To our knowledge, this is the first quantitative and qualitative prediction introducing this normalization, which further estimates particle trapping positions within <10% error in DC-iDEP requiring no $C$ factors. We note, however, that 5.1 $\mu$m particles present the largest experimental deviation from the predictions (9.15%), which is also evidenced in Figure 3e.

Our results demonstrate that the common assumption of negligible surface conductance in insulator-based EK has two important consequences. First, $\sigma_p \sim 0$ leads to an independence of the DC polarizability on particle and medium properties, as $f_{CM} = -1/2$.[11,22,44,45] This implies that, if linear EK models are used, any variability in $\mathbf{u}_{DEP}$ (other than $\nabla(\mathbf{E}\cdot\mathbf{E})$) will be attributed to size effects only. Second, in addition to precluding any possible particle characterization, it ignores the accentuated effect that surface conductance has on smaller particles, since $\sigma_p \sim 1/a$ in eq 10.[34] By contrast, the current nonlinear theory explains the dependence of trapping through $E_{EEC}$ of a particle, which can still be explicitly linked to its physical properties by means of eq 7. For instance, this approach has potential for providing an EK signature for biological cells.[46] As seen in Table 1, the current model proposes $\sigma_p \neq 0$ and even $\sigma_m < \sigma_p$ in the case of 1.0 $\mu$m. This result is in agreement with AC-eDEP measurements, which assert $f_{CM} > 0$ for charged dielectric particles at low frequencies and low $\sigma_m$,[26] as opposed to the typical DC-iDEP assessment of negative DEP for those conditions.

Because the observed errors are still within <10%, we recall the several approximations presently taken: (1) thin EDL; (2) electric field intensity range and Du limits; (3) small spatial variation of $\mathbf{E}$ when compared with $a$ and $\kappa^{-1}$; (4) 2D geometry; (5) linear EOF; and (6) neglect of permanent medium changes. Assumptions (1) and (2) relate to $a$ and $\rho_q$, while (3−6) impact device geometry and EK properties. While bigger particles typically guarantee (1) is satisfied, (2) will limit the range of applicable fields (smaller $\beta$, and thus, particles experience nonlinear EK at weaker fields). At the same time, bigger particles lead to smaller Du numbers, provided $\zeta_0 \gtrsim 1$, allowing analysis by arbitrary field theories (see range of validity of solutions of the SY model in Ref 4.). Conversely, increasing $a$ affects assumptions (3−4) because the particle's dielectric nature locally distorts the electric field, potentially invalidating a 2D approximation of eq 8. The extent of this effect was not accounted for in the theory and should be the subject of future studies, as it could potentially explain the larger deviations found for the biggest particles here tested; $a \sim H$ and $a \sim G$ could similarly invalidate assumption (3) due to wall effects, but we note that in the case of 5.1 $\mu$m particles traveling through the center of the gap, the distance to the nearest wall would still be much greater than $\kappa^{-1}$. Moreover, a prolonged and intense $E_0$ produces nonlinear electrothermal flow (ETF),[47] pH and electrolyte alterations by faradaic processes,[48] and permanent surface chemistry changes,[49] affecting assumptions (5) and (6). In our DC setup, however, we used diluted media ($\sigma_m < 10$ $\mu$S cm$^{-1}$) and relatively short high-voltage applications (10 s) to prevent Joule heating. Previous experiments from our group demonstrated that uniform DC fields on the same microchannels without posts require higher conductivities ($\sigma_m \sim 150$ $\mu$S cm$^{-1}$) and $E_0$= 2500 V cm$^{-1}$ to generate $\Delta T \sim 10$ K.[35] Other studies on microfluidic channels featuring highly nonuniform fields confirm that DC biases of 1000 V and $\sigma_m = 100$ $\mu$S cm$^{-1}$ produce marginal temperature rises ($\Delta T \sim 2$ K).[50]

The application of high DC inevitably leads to presently unaccounted-for electrochemical processes (e.g., electrolysis). In our design, large reservoirs mitigate migration of electro-


https://dx.doi.org/10.1021/acs.analchem.0c01303
Anal. Chem. 2020, 92, 12871−12879

chemical products into the channel,[40,53] significantly reduce pH changes that normally take minutes to develop,[48] and prevent pressure-driven backflow. Nonetheless, we warrant small pH changes are bound to occur to an extent, likely acting to reduce EOF. However, as demonstrated by the high bias experiments (2000 V $cm^{-1}$), negative EK velocities are swiftly established (<50 ms), suggesting that diffusion and migration-driven bulk electrochemical changes are not responsible for the observed phenomena. We recommend that future studies maximize reservoir volume and minimize $E_0$, both in magnitude and duration, to effectively isolate the nonlinear velocity components. Yet, because this approach might be impractical for microfluidics applications, we expect that an adaption of the current methodology could be required, either through experimental pH control or by introducing a modified version of the theory.

## CONCLUSIONS

In this study, the tested carboxylated particles reversed their EK velocity direction when subjected to a sufficiently strong DC uniform field of magnitude $E_{EEC}$. This result, which cannot be predicted by linear EK theory, points to the plausibility of higher-order phenomena connected to surface conductance interfacial effects occurring at nonzero Du and extreme conditions, that is, high electric fields that distort the uniformity of the EDL. Here, we have connected the SY theory of nonlinear EK with our experimental observations as an exploratory model and have demonstrated how it plausibly accounts for the measured $u_p$ component that counterbalances EOF. Furthermore, the application of the presented nonlinear EK model under nonuniform fields allowed us to forecast the experimentally obtained $E_{trap}$ values of particles, as well as their trap locations. Although the $E_{EEC}$ prediction mechanism resulted in errors between 5.91 and 9.15%, it remarkably required no physically unaccounted for correction factors.

In addition to providing a more in-depth understanding of the physics involved in particle trapping, the presented model suggests future directions for device designs. For instance, the calculated particle trap locations indicate that the introduced dielectric constrictions act to spatially map the $E_{EEC}$ threshold field into a device. This implies emphasis should be placed on matching the field magnitudes to that threshold value through careful design of the amplification factor, rather than on increasing $\nabla(\mathbf{E}\cdot\mathbf{E})$, as has been the common practice. Optimizing the DC field-independent amplification factor in this way, for a fixed DC bias, will reduce the high voltage requirements needed to achieve particle trapping. This will bring the technology closer to its integration with portable electronic instrumentation, making it an amenable tool for point of care applications.

## ASSOCIATED CONTENT

### Supporting Information

The Supporting Information is available free of charge at https://pubs.acs.org/doi/10.1021/acs.analchem.0c01303.

Experimental setup; voltage application sequence; bipolar coordinate system; COMSOL geometries and simulations; channel geometries and trapping predictions; linear EK models; model parameters; and plot of particle velocity at high conductivity for 5.1 $\mu$m particles (PDF)

EK velocity and trapping videos for 1.0 $\mu$m particles (MP4)

EK velocity and trapping videos for 1.9 $\mu$m particles (MP4)

EK velocity and trapping videos for 5.1 $\mu$m particles (MP4)

EK response of all tested particles at 2000 V $cm^{-1}$ (MP4)

## AUTHOR INFORMATION


### Corresponding Author

**Victor H. Perez-Gonzalez** − *School of Engineering and Sciences, Tecnologico de Monterrey, Monterrey, Nuevo Leon 64849, Mexico;* orcid.org/0000-0003-4503-7774; Email: vhpg@tec.mx

### Authors

**Braulio Cardenas-Benitez** − *School of Engineering and Sciences, Tecnologico de Monterrey, Monterrey, Nuevo Leon 64849, Mexico*

**Binny Jind** − *School of Engineering and Sciences, Tecnologico de Monterrey, Monterrey, Nuevo Leon 64849, Mexico*

**Roberto C. Gallo-Villanueva** − *School of Engineering and Sciences, Tecnologico de Monterrey, Monterrey, Nuevo Leon 64849, Mexico;* orcid.org/0000-0002-7553-1039

**Sergio O. Martinez-Chapa** − *School of Engineering and Sciences, Tecnologico de Monterrey, Monterrey, Nuevo Leon 64849, Mexico;* orcid.org/0000-0003-2689-1166

**Blanca H. Lapizco-Encinas** − *Microscale Bioseparations Laboratory, Rochester Institute of Technology, Rochester, New York 14623, United States;* orcid.org/0000-0001-6283-8210

Complete contact information is available at: https://pubs.acs.org/10.1021/acs.analchem.0c01303


### Author Contributions

B.C.-B contributed to methodology, formal analysis, investigation, data curation, and visualization of the study, wrote the original draft, and reviewed and edited the manuscript. B.J. contributed to methodology, investigation, visualization, and validation of the study and reviewed and edited the manuscript. R.C.G.-V. contributed to validation of the study and reviewed and edited the manuscript. S.O.M.-C. contributed to funding acquisition, obtained resources, and reviewed and edited the manuscript. B.H.L.-E. contributed to project administration and visualization of the study, wrote original draft, and reviewed and edited the manuscript. V.H.P.-G. contributed to conceptualization, project administration, and supervision of the study, wrote original draft, and reviewed and edited the manuscript.

### Notes

The authors declare no competing financial interest.

## ACKNOWLEDGMENTS

The authors acknowledge the financial support provided by the Nano-Sensors & Devices Research Group (0020209I06) and the Federico Baur Endowed Chair in Nanotechnology (0020240I03) at Tecnologico de Monterrey. Additional financial support is provided by the National Science Foundation (Award CBET-1705895). The authors acknowledge Alejandro Lujambio for suggesting the use of bipolar coordinates in the solution.

## REFERENCES


(1) Bazant, M. Z.; Kilic, M. S.; Storey, B. D.; Ajdari, A. *Adv. Colloid Interface Sci.* **2009**, *152*, 48−88.
(2) Dukhin, S. S. *Adv. Colloid Interface Sci.* **1991**, *36*, 219−248.
(3) Mishchuk, N. A.; Takhistov, P. V. *Colloids Surf A Physicochem. Eng. Asp.* **1995**, *95*, 119−131.
(4) Schnitzer, O.; Yariv, E. *Phys. Fluids* **2014**, *26*, 122002.
(5) Schnitzer, O.; Zeyde, R.; Yavneh, I.; Yariv, E. *Phys. Fluids* **2013**, *25*, No. 052004.
(6) Zhan, X.; Wang, J.; Xiong, Z.; Zhang, X.; Zhou, Y.; Zheng, J.; Chen, J.; Feng, S.-P.; Tang, J. *Nat. Commun.* **2019**, *10*, 3921.
(7) Dukhin, S. S. *Adv. Colloid Interface Sci.* **1993**, *44*, 1−134.
(8) Xuan, X. *Electrophoresis* **2019**, *40*, 2484−2513.
(9) Wang, Q.; Jones, A. A. D.; Gralnick, J. A.; Lin, L.; Buie, C. R. *Sci. Adv.* **2019**, *5*, No. eaat5664.
(10) Crowther, C. V.; Sanderlin, V.; Hayes, M. A.; Gile, G. H. *Analyst* **2019**, *144*, 7478−7488.
(11) Gallo-Villanueva, R.; Pérez-González, V. H.; Davalos, R.; Lapizco-Encinas, B. H. *Electrophoresis* **2011**, *32*, 2456−2465.
(12) Lapizco-Encinas, B. H. *Electrophoresis* **2019**, *40*, 358−375.
(13) Hilton, S. H.; Hayes, M. A. *Anal. Bioanal. Chem.* **2019**, *411*, 2223.
(14) Crowther, C. V.; Hayes, M. A. *Analyst* **2017**, *142*, 1608−1618.
(15) Hill, N.; Lapizco-Encinas, B. H. *Electrophoresis* **2019**, *40*, 2541−2552.
(16) Zhu, J. J.; Xuan, X. C. J. *Colloid Interface Sci.* **2009**, *340*, 285−290.
(17) Zhu, J. J.; Tzeng, T. R. J.; Hu, G. Q.; Xuan, X. C. *Microfluid. Nanofluid.* **2009**, *7*, 751−756.
(18) Church, C.; Zhu, J.; Xuan, X. *Electrophoresis* **2011**, *32*, 527−531.
(19) Patel, S.; Showers, D.; Vedantam, P.; Tzeng, T.-R.; Qian, S.; Xuan, X. *Biomicrofluidics* **2012**, *6*, No. 034102.
(20) Kale, A.; Patel, S.; Xuan, X. *Micromachines* **2018**, *9*, 123.
(21) Kang, K. H.; Xuan, X.; Kang, Y.; Li, D. J. *Appl. Phys.* **2006**, *99*, 064702−064708.
(22) Li, M.; Li, S.; Cao, W.; Li, W.; Wen, W.; Alici, G. *J. Micromech. Microeng.* **2012**, *22*, No. 095001.
(23) Saucedo-Espinosa, M. A.; Lapizco-Encinas, B. H. *Electrophoresis* **2015**, *36*, 1086−1097.
(24) Mohammadi, M.; Zare, M. J.; Madadi, H.; Sellarès, J.; Casals-Terré, J. *Anal. Bioanal. Chem.* **2016**, *408*, 5285−5294.
(25) Mohammadi, M.; Madadi, H.; Casals-Terré, J.; Sellarès, J. *Anal. Bioanal. Chem.* **2015**, 1−12.
(26) Chen, Q.; Yuan, Y. *J. RSC Adv.* **2019**, *9*, 4963−4981.
(27) Baylon-Cardiel, J. L.; Lapizco-Encinas, B. H.; Reyes-Betanzo, C.; Chávez-Santoscoy, A. V.; MartÌnez-Chapa, S. O. *Lab Chip* **2009**, *9*, 2896−2901.
(28) Nakano, A.; Camacho-Alanis, F.; Ros, A. *Analyst* **2015**, *140*, 860−868.
(29) Liu, Y.; Jiang, A.; Kim, E.; Ro, C.; Adams, T.; Flanagan, L. A.; Taylor, T. J.; Hayes, M. A. *Analyst* **2019**, *144*, 4066−4072.
(30) Shirahama, H.; Suzawa, T. *Polym. J.* **1984**, *16*, 795−803.
(31) Kirby, B. J. *Micro- and Nanoscale Fluid Mechanics: Transport in Microfluidic Devices*; Cambridge University Press, 2010.
(32) Feng, H.; Wong, T. N. *Int. J. Heat Mass Transfer* **2015**, *88*, 674−683.
(33) Mark, J. E. *Polymer data handbook*; Oxford university press, 2009.
(34) Ermolina, I.; Morgan, H. J. *Colloid Interface Sci.* **2005**, *285*, 419−428.
(35) Gallo-Villanueva, R. C.; Perez-Gonzalez, V. H.; Cardenas-Benitez, B.; Jind, B.; Martinez-Chapa, S. O.; Lapizco-Encinas, B. H. *Electrophoresis* **2019**, *40*, 1408−1416.
(36) Tatsumi, K.; Nishitani, K.; Fukuda, K.; Katsumoto, Y.; Nakabe, K. *Meas. Sci. Technol.* **2010**, *21*, 105402.
(37) Von Smoluchowski, M. *Bull. Akad. Sci. Cracovie.* **1903**, *8*, 182−200.
(38) Perez-Gonzalez, V. H.; Gallo-Villanueva, R. C.; Cardenas-Benitez, B.; Martinez-Chapa, S. O.; Lapizco-Encinas, B. H. *Anal. Chem.* **2018**, *90*, 4310−4315.
(39) Mata-Gómez, M. A.; Gallo-Villanueva, R. C.; González-Valdez, J.; Martínez-Chapa, S. O.; Rito-Palomares, M. *Electrophoresis* **2016**, *37*, 519−528.
(40) Saucedo-Espinosa, M. A.; Lapizco-Encinas, B. H. *Biomicrofluidics* **2016**, *10*, No. 033104.
(41) Kirby, B. J.; Hasselbrink, E. F., Jr. *Electrophoresis* **2004**, *25*, 203−213.
(42) Arnold, W. M.; Schwan, H. P.; Zimmermann, U. J. *Phys. Chem.* **1987**, *91*, 5093−5098.
(43) Bastos-GonzáLez, D.; Ortega-Vinuesa, J. L.; Lasnieves, D. F. J.; Hidalgo-ÁLvarez, R. J. *Colloid Interface Sci.* **1995**, *176*, 232−239.
(44) Barbulovic-Nad, I.; Xuan, X.; Lee, J. S. H.; Li, D. *Lab Chip* **2006**, *6*, 274−279.
(45) Regtmeier, J.; Eichhorn, R.; Viefhues, M.; Bogunovic, L.; Anselmetti, D. *Electrophoresis* **2011**, *32*, 2253−2273.
(46) Coll De Peña, A.; Miller, A.; Lentz, C. J.; Hill, N.; Parthasarathy, A.; Hudson, A. O.; Lapizco-Encinas, B. H. *Anal. Bioanal. Chem.* **2020**, *412*, 3935−3945.
(47) Wang, Q.; Dingari, N. N.; Buie, C. R. *Electrophoresis* **2017**, *38*, 2576−2586.
(48) Gencoglu, A.; Camacho-Alanis, F.; Nguyen, V. T.; Nakano, A.; Ros, A.; Minerick, A. R. *Electrophoresis* **2011**, *32*, 2436−2447.
(49) Squires, T. M. *Lab Chip* **2009**, *9*, 2477−2483.
(50) Nakano, A.; Luo, J.; Ros, A. *Anal. Chem.* **2014**, *86*, 6516−6524.
(51) Ozuna-Chacón, S.; Lapizco-Encinas, B. H.; Rito-Palomares, M.; Martínez-Chapa, S. O.; Reyes-Betanzo, C. *Electrophoresis* **2008**, *29*, 3115−3122.
(52) LaLonde, A.; Gencoglu, A.; Romero-Creel, M. F.; Koppula, K. S.; Lapizco-Encinas, B. H. *J Chromatogr A* **2014**, *1344*, 99−108.
(53) Novotný, T.; Gaš, B. *Electrophoresis* 2019.



https://dx.doi.org/10.1021/acs.analchem.0c01303
*Anal. Chem.* 2020, 92, 12871−12879